

# The Implicit Biases of Stochastic Gradient Descent on Deep Neural Networks with Batch Normalization

Ziquan Liu Yufei Cui Jia Wan Yu Mao Antoni B. Chan

Department of Computer Science  
City University of Hong Kong

{ziquanliu2-c, yufeicui3-c, jiawan6-c, yuamao7-c}@my.cityu.edu.hk, abchan@cityu.edu.hk

## Abstract

Deep neural networks with batch normalization (BN-DNNs) are invariant to weight rescaling due to their normalization operations. However, using weight decay (WD) benefits these weight-scale-invariant networks, which is often attributed to an increase of the effective learning rate when the weight norms are decreased. In this paper, we demonstrate the insufficiency of the previous explanation and investigate the implicit biases of stochastic gradient descent (SGD) on BN-DNNs to provide a theoretical explanation for the efficacy of weight decay. We identify two implicit biases of SGD on BN-DNNs: 1) the weight norms in SGD training remain constant in the continuous-time domain and keep increasing in the discrete-time domain; 2) SGD optimizes weight vectors in fully-connected networks or convolution kernels in convolution neural networks by updating components lying in the input feature span, while leaving those components orthogonal to the input feature span unchanged. Thus, SGD without WD accumulates weight noise orthogonal to the input feature span, and cannot eliminate such noise. Our empirical studies corroborate the hypothesis that weight decay suppresses weight noise that is left untouched by SGD. Furthermore, we propose to use weight rescaling (WRS) instead of weight decay to achieve the same regularization effect, while avoiding performance degradation of WD on some momentum-based optimizers. Our empirical results on image recognition show that regardless of optimization methods and network architectures, training BN-DNNs using WRS achieves similar or better performance compared with using WD. We also show that training with WRS generalizes better compared to WD, on other computer vision tasks.

## 1. Introduction

Because of its benefits to training and generalization, batch normalization (BatchNorm, BN) [22] has become

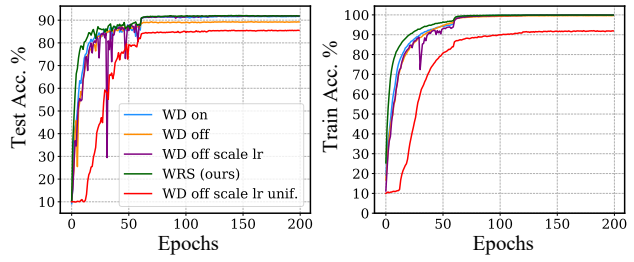


Figure 1. Test accuracy of VGG16 on CIFAR10 using various regularization schemes: weight decay (WD), weight rescaling (WRS), learning rate scaling (scale LR). Training with WRS converges faster than WD and LR scaling, with similar test accuracy to WD, even though WRS does not increase effective learning rate.

a standard component in modern neural networks and is employed in numerous computer vision tasks, e.g., image recognition [18], semantic segmentation [7] and object detection [41]. Despite being widely used, BN is still not well-understood in many aspects. One mystery about deep neural networks with BN (BN-DNNs) is *why such a neural network, which is invariant to scaling of its weights, is affected by weight decay (WD)*, an explicit regularization controlling the  $l_2$  norms of weights (denoted as *weight norms*). Previous works [50, 19, 26] hypothesize that weight-scale invariant networks, including networks with BN and WeightNorm [42], need penalties on the weight norms to increase the effective learning rate, resulting in a faster convergence and better generalization ability [27]. In this paper, we demonstrate that the effective learning rate argument cannot fully explain the effect of weight decay in weight-scale invariant networks. We propose to understand the dynamics of weights during training and the effect of  $l_2$  regularization by investigating implicit biases of stochastic gradient descent (SGD) on BN-DNNs. Our theoretical analysis is validated by empirical studies on standard neural architectures and datasets. By unveiling the intrinsic properties of their training dynamics, we take a step towards a more principled understanding of BN-DNNs.

Specifically, we identify two kinds of implicit biases of SGD on BN-DNNs. First, we prove that the gradient flow [11, 2] of a BN-DNN without WD keeps the weight norms constant during training. In other words, weights in a BN-DNN have the same scales throughout training if we set an infinitesimal learning rate. In contrast, when weight decay is used, the weight norm follows an exponential decay in time (or optimization step). In the discrete-time domain, we show that the weight norm is always increased in a BN-DNN without WD. Second, we prove that SGD on BN-DNNs updates components of the weight vector that are inside the span of input features, while ignoring those components orthogonal to the span (the weight vector has the same dimension as the input). According to [16, 1], the intrinsic dimensionality of feature representations in DNNs is substantially lower than that of the ambient space. Thus if a weight vector has noise lying in the orthogonal subspace of its input feature span, SGD cannot effectively remove that noise without weight regularization. Based on this observation, we provide an explanation for the phenomenon that using a larger learning rate has a similar effect as WD [19]. Furthermore, we propose a weight rescaling (WRS) scheme to shrink those noise lying in the orthogonal input space as an alternative to WD, which avoids the negative effect of WD on some optimizers, e.g. Adam [23, 32].

In summary, the contributions of this paper are 3-fold: 1) we discover the implicit biases of SGD on weights of BN-DNNs; 2) we give a theoretical explanation on the effect of WD on BN-DNNs based on these implicit biases, and provide empirical evidence; 3) we propose to regularize a BN-DNN with WRS instead of WD when using complex optimizers, and demonstrate the advantages of WRS over WD in various computer vision tasks, architectures and datasets.

## 2. Related Work

We discuss previous work on understanding the dynamics of BN-DNN and explanations on why WD is beneficial to the generalization of BN-DNNs.

### 2.1. Training Dynamics of BatchNorm Networks

[33] investigates the learning dynamics of BN-DNNs using ordinary differential equations (ODE), and shows that BN-DNNs can use a larger learning rate to optimize an empirical risk function than DNNs without BN. In contrast, in our paper we consider the dynamics of  $l_2$ -norm in BN-DNNs and give ODEs of  $l_2$  norms in the continuous-time domain. Our analysis on the  $l_2$  norms together with the low-rank optimization property of SGD motivates the proposal of WRS regularization.

[48] uses the mean-field theory to demonstrate that vanilla BN-DNNs without residual connections cannot be trained as a result of the gradient explosion at initialization. They also study the learning dynamics of BN-DNNs, and

empirically show that even if the initial gradients tend to explode, both  $l_2$  norms and gradients remain stable after the initial optimization stage. Building on their empirical result, our paper theoretically explains why the equilibrium happens in BN-DNNs by deriving the ODEs of weight norms and further investigates the impact of SGD on weights from the perspective of input features.

[6] empirically shows that BN’s faster convergence and better generalization are due to larger learning rates, while [43] argues that BN’s benefit is not relevant to the internal covariate shift, and shows that BN makes the loss landscape smoother compared to without BN. In our paper, we also consider the optimization dynamics of BN-DNNs, but we focus on weight norms and sparse structures of weights.

### 2.2. WD on Weight-Scaling-Invariance Networks

[46] is the first work to investigate the relationship between  $l_2$  regularization and normalization in DNNs. They show that the weight norm is determined by the hyperparameter in  $l_2$  regularization and the learning rate, but the relationship between weight norm and generalization is not considered. They also propose to scale weights to the unit norm during training. The difference is that we derive WRS regularization from the perspective of implicit biases of SGD and show the effect of weight rescaling on the generalization and optimization of BN-DNNs, while [46] proposes this scaling to keep the learning rate stable. In addition, our analysis validates the crucial assumption in [46] that the weight norm remains constant as training converges.

[19, 50] explain the effect of WD on the generalization of BN-DNNs via an effective learning rate. We replicate the experiment in [19] that seemingly validates the effective learning rate explanation and point out the imperfection of this validation. [19] proposes to fix the weight *matrix* norm during training, but their bounded WeightNorm (BWN) is based on WeightNorm instead of BN and their motivation is still the effective learning rate. In contrast, the proposed WRS renormalizes weight *vectors* in a BN-DNN and is based on implicit biases of SGD. Our empirical study demonstrates the benefit of WRS over BWN in terms of generalization and training stability. [31] proposes an alternative to WD that avoids the weight-scale-shifting-invariance effect in standard neural networks with ReLU activations, achieving better adversarial robustness than WD. However, the regularization minimizes a product of all weight norms and causes unbalanced weight norms in different layers, which impedes the optimization [36] and hurts generalization. In contrast, our WRS balances weight norms at different layers and improves generalization. [20] proposes the weight rescaling in BN-DNNs to avoid the negative effect of scaling-based symmetry of weight space. Our paper shows that a BN-DNN does not have the unbalanced weights effect during optimization since the weight

norm does not change drastically based on Theorem 3.1. Moreover, [20] does not find WRS can totally replace WD and still use both WRS and WD but our paper provides a new explanation on the effect of WD on BN-DNNs, which inspires us to use WRS as an alternative to WD when training NNs with advanced optimizers. Both Weight Standardization (WS) [38] and WRS makes the weight norms stable during training, but the difference is that our work focuses on explaining the effect of WD from the perspective of weight norm dynamics and proposes to replace WD with WRS to achieve better generalization.

A classic paper [25] investigates the effect of WD on a one-layer NN by projecting weights onto the input space. Our paper extends [25] to a BN-DNN setting, and gives empirical studies on modern NN. [4] investigates the benign overfitting phenomenon in linear regression by studying the data covariance matrix, which is similar to our analysis on the input feature covariance matrix. However, our focus is on more complex DNNs. Finally, our analysis on the input feature span is closely related to kernel methods [5]. In kernel methods, SGD/GD initialized outside the span of kernel features cannot converge to the minimum norm solution since the components orthogonal to the input space are not updated. We show that SGD for a BN-DNN without regularizing on the components orthogonal to the input feature span cannot converge to a solution with succinct weights.

### 3. Dynamics of Weight Norms in BN-DNNs

In this section we introduce notations of a BN-DNN and analyze the weight norm dynamics during SGD optimization in both continuous-time and discrete-time domains. Here we perform the analysis on a fully-connected network, and a similar analysis on convolution neural networks is presented in the Supplemental A.5.

#### 3.1. BatchNorm Deep Neural Network (BN-DNN)

A BN-DNN is denoted as  $f_{\Theta} : \mathbb{R}^D \mapsto \mathbb{R}^K$ , where  $D$  is the dimension of an input sample  $\mathbf{x}_i$  and  $K$  is the number of classes in classification or the dimension of output in regression. The input  $\mathbf{X} = \{\mathbf{x}_i\}_{i=1}^N$  and label  $\mathbf{Y} = \{\mathbf{y}_i\}_{i=1}^N$  are sampled from an unknown distribution  $\mathcal{D}$ . We assume that the BN-DNN is composed of a number of BN layers, comprising a sequence of weight multiplication, batch normalization and activation function [22]. The BN layer is

$$\mathbf{h}_{l+1}^{(i)} = \phi(\mathcal{BN}(\mathbf{W}_l^T \mathbf{h}_l^{(i)})), \quad (1)$$

where  $\mathbf{h}_l^{(i)} \in \mathbb{R}^{H_l \times 1}$  is the  $i$ th hidden variable of  $l$ th layer,  $\mathbf{W}_l \in \mathbb{R}^{H_l \times H_{l+1}}$  is the weight matrix of  $l$ th layer,  $\mathcal{BN}$  represents the BatchNorm operation,  $\phi(x)$  is the ReLU activation function, and we define the input as  $\mathbf{h}_0^{(i)} = \mathbf{x}_i$ . The

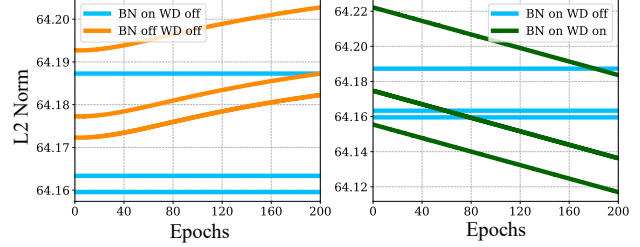


Figure 2.  $l_2$  weight norms during training for: 1) BN on (blue), 2) BN off (yellow) and 3) BN on and WD on (green). BN forces weight norms to be constant, while using WD decreases weight norms as an exponential function (here appearing locally linear).

BatchNorm operation is an element-wise operation,

$$\hat{\mathbf{h}}_{l+1,j}^{(i)} = \mathcal{BN}(\mathbf{W}_{l,j}^T \mathbf{h}_l^{(i)}) = \gamma_{l,j} \frac{\mathbf{W}_{l,j}^T \mathbf{h}_l^{(i)} - \mathbf{W}_{l,j}^T \boldsymbol{\mu}_l^{(B)}}{\|\mathbf{W}_{l,j}\|_{\Sigma_l^{(B)}}} + \beta_{l,j}$$

where  $\|\mathbf{W}_{l,j}\|_{\Sigma_l^{(B)}} = (\mathbf{W}_{l,j}^T \Sigma_l^{(B)} \mathbf{W}_{l,j})^{1/2}$  is the standard deviation of this neuron's output and we use  $t_{l,j}^{(i)}$  to denote the normalized output, i.e.  $\hat{\mathbf{h}}_{l+1,j}^{(i)} = \gamma_{l,j} t_{l,j}^{(i)} + \beta_{l,j} \cdot \boldsymbol{\mu}_l^{(B)}$  and  $\Sigma_l^{(B)}$  are the mean and covariance matrix of the current batch,

$$\boldsymbol{\mu}_l^{(B)} = \frac{1}{B} \sum_{i=1}^B \mathbf{h}_l^{(i)}, \quad \Sigma_l^{(B)} = \frac{1}{B} \sum_{i=1}^B \mathbf{h}_l^{(i)} \mathbf{h}_l^{(i)T} - \boldsymbol{\mu}_l^{(B)} \boldsymbol{\mu}_l^{(B)T}.$$

Note that the covariance matrix  $\Sigma_l^{(B)}$  is a result of variance calculation and does not violate the i.i.d. assumption of BatchNorm. Let there be  $L$  BN layers and one output layer in the network, i.e.  $\Theta = \{\mathbf{W}_0, \dots, \mathbf{W}_L\}$  where  $\mathbf{W}_L \in \mathbb{R}^{H_L \times K}$ . The network is trained with mini-batch SGD to minimize the empirical risk  $R$  over dataset  $\{\mathbf{X}, \mathbf{Y}\}$ , where  $R$  can be cross-entropy or mean squared error,

$$\Theta^* = \min_{\Theta} \mathcal{R}_{\Theta}(\mathbf{X}, \mathbf{Y}) = \min_{\Theta} \frac{1}{N} \sum_{i=1}^N r(f_{\Theta}(\mathbf{x}_i), \mathbf{y}_i), \quad (2)$$

where  $r(f_{\Theta}(\mathbf{x}_i), \mathbf{y}_i)$  is written as  $r^{(i)}$  for short. The  $l_2$  norm of a vector is denoted as  $\|\cdot\|_2$  and the Frobenius norm of a matrix is denoted as  $\|\cdot\|_F$ .

#### 3.2. Continuous-Time Analysis

The research into gradient flow, i.e., SGD with an infinitesimal learning rate, provides insights on the optimization of DNNs [11, 2]. Inspired by the previous work [10] on the gradient flow of weight norms in a standard ReLU-DNN, we analyze the differential equation of weight norms in a BN-DNN. According to the chain rule, the gradient flow of the  $l_2$  norm of weight vector  $\mathbf{W}_{l,j}(t)$  is

$$\frac{d\|\mathbf{W}_{l,j}(t)\|_2^2}{dt} = 2\langle \mathbf{W}_{l,j}(t), \frac{d\mathbf{W}_{l,j}(t)}{dt} \rangle. \quad (3)$$

Because we use SGD, the gradient flow of  $\mathbf{W}_{l,j}(t)$  follows the negative direction of the gradient of loss w.r.t.  $\mathbf{W}_{l,j}(t)$ ,

$$\frac{d\mathbf{W}_{l,j}(t)}{dt} = -\frac{\partial R_{\Theta(t)}(\mathbf{X}^{(B)}, \mathbf{Y}^{(B)})}{\partial \mathbf{W}_{l,j}(t)}.$$

By deriving the gradient of the loss w.r.t.  $\mathbf{W}_{l,j}(t)$ , we have the following theorem.

**Theorem 3.1** Given a network as in Sec. 3.1, which is trained using SGD to minimize the loss  $R_{\Theta}$ , the gradient flow of the weight norms in BN layers is zero,

$$\frac{d\|\mathbf{W}_{l,j}(t)\|_2^2}{dt} = 0. \quad (4)$$

*Proof.* In one step of SGD, we calculate the gradient of  $\mathbf{W}_{l,j}(t)$  using a mini batch  $(\mathbf{X}^{(B)}, \mathbf{Y}^{(B)}) = \{\mathbf{x}_i, \mathbf{y}_i\}_{i=1}^B$ ,

$$\frac{\partial R_{\Theta(t)}(\mathbf{X}^{(B)}, \mathbf{Y}^{(B)})}{\partial \mathbf{W}_{l,j}(t)} = \sum_{i=1}^B \frac{\partial r^{(i)}(t)}{\partial \hat{h}_{l+1,j}^{(i)}(t)} \frac{\partial \hat{h}_{l+1,j}^{(i)}(t)}{\partial \mathbf{W}_{l,j}(t)}.$$

Then the second gradient term  $\partial \hat{h}_{l+1,j}^{(i)}(t)/\partial \mathbf{W}_{l,j}(t)$  is

$$\gamma_{l,j} \left[ \frac{\mathbf{h}_l^{(i)} - \boldsymbol{\mu}_l^{(B)}}{\|\mathbf{W}_{l,j}\|_{\Sigma_l^{(B)}}} - \frac{\mathbf{W}_{l,j}^T(\mathbf{h}_l^{(i)} - \boldsymbol{\mu}_l^{(B)})}{\|\mathbf{W}_{l,j}\|_{\Sigma_l^{(B)}}^3} \Sigma_l^{(B)} \mathbf{W}_{l,j} \right], \quad (5)$$

where  $t$  is omitted for clarity. It is easy to show that  $\langle \mathbf{W}_{l,j}(t), \partial \hat{h}_{l+1,j}^{(i)}(t)/\partial \mathbf{W}_{l,j}(t) \rangle = 0$ , and substituting into (3) gives (4) (see Supp. A.1 for the complete proof).

There are several implications of Theorem 3.1. First, when the learning rate is infinitesimal, the weight norms in BN layers remain the same as their initializations. Second, in the continuous-time domain, the weight in a BN layer only changes its direction and the scaling is controlled by another parameter  $\gamma_{l,j}$ , which is the same as WeightNorm [42]. Third, as the following corollary shows, using WD in this domain leads to an exponential decay of weight norm. We note that [37] shows that gradients are orthogonal to weights in their DDP-Normalization, which normalizes a weight by the output's sample variance to control complexity. However, [37] focuses on regularizing *data-dependent* complexity measure in DNNs, while our paper investigates *data-independent* WD in BN-DNNs through the dynamics of weight norms, and we propose to replace WD with WRS based on SGD's implicit biases.

**Corollary 3.2** Given a network as in Sec. 3.1 and the network is trained using gradient descent to minimize the loss  $R_{\Theta}$  and  $l_2$  regularization  $\frac{\lambda}{2} \sum_{l=0}^L \|\mathbf{W}_l\|_F^2$ , then the weight norm in a BN layer follows an exponential decay,

$$\|\mathbf{W}_{l,j}(t)\|_2^2 = \|\mathbf{W}_{l,j}(0)\|_2^2 \exp(-2\lambda t). \quad (6)$$

See the Supp. A.2 for the proof. Fig. 2 shows an example of decaying weight norms due to WD. The exponential decay of WD indicates that the gradient flow of SGD with WD leads to shrinking weight norms, and the optimal solution is weights with zero norm. Thus, the dynamics lead

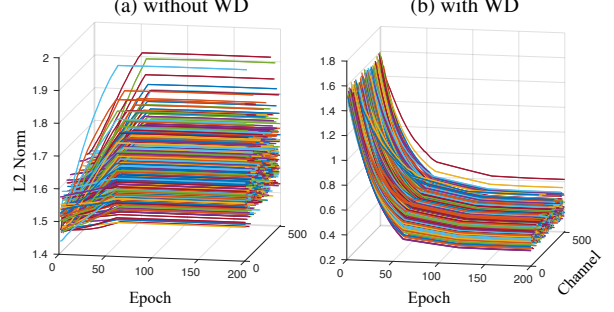


Figure 3. Weight norms during training of a BN-DNN. Each line denotes the  $l_2$  norm of one output channel. (a) Without WD, weight norms increases at early epochs and remain stable afterwards, when the learning rate is decayed. (b) With WD, the decrease of weight norms look like exponential functions.

to a degenerate solution, and may cause poor optimization procedures. To address this issue, we propose a better training scheme, WRS, that has the same regularizing effect and does not lead to degenerate solutions.

### 3.3. Discrete-Time Analysis

We next analyze the change of weight norms when a relatively large learning rate is used in SGD. Instead of deriving an ordinary differential equation for the weight norm, we investigate the difference between the weight norms of two consecutive optimization steps, i.e.  $\Delta_{l,j}(t) = \|\mathbf{W}_{l,j}(t+1)\|_2^2 - \|\mathbf{W}_{l,j}(t)\|_2^2$ . Let the learning rate be  $\eta(t)$ , then  $\mathbf{W}_{l,j}(t+1)$  is obtained by one step of gradient descent,

$$\mathbf{W}_{l,j}(t+1) = \mathbf{W}_{l,j}(t) - \eta(t) \frac{\partial R_{\Theta(t)}(\mathbf{X}^{(B)}, \mathbf{Y}^{(B)})}{\partial \mathbf{W}_{l,j}(t)}.$$

The proof of Theorem 3.1 shows that the inner product between  $\mathbf{W}_{l,j}(t)$  and  $\partial R_{\Theta(t)}(\mathbf{X}^{(B)}, \mathbf{Y}^{(B)})/\partial \mathbf{W}_{l,j}(t)$  is zero. Thus we have the following corollary.

**Corollary 3.3** Given network as in Sec. 3.1 and the network is trained by SGD to minimize  $R_{\Theta}(\mathbf{X}, \mathbf{Y})$ , we have

$$\Delta_{l,j}(t) = \eta(t)^2 \left\| \frac{\partial R_{\Theta(t)}(\mathbf{X}^{(B)}, \mathbf{Y}^{(B)})}{\partial \mathbf{W}_{l,j}(t)} \right\|_2^2. \quad (7)$$

When the learning rate  $\eta(t)$  goes to infinitesimal, the training enters the continuous-time domain and Theorem 3.1 holds, i.e.  $\Delta_{l,j}(t) \rightarrow 0$ . The corollary shows that in practice the weight norm always increases and the amount of increase is determined by the magnitude of its gradient and the learning rate. This corollary validates the intuition that weight norms will go unbounded in a BN-DNN [19, 46], and provides a quantitative increasing rate for weight norms. Fig. 3 shows the change of norms in one convolution layer of VGG16 [44]<sup>1</sup>, where each line denotes

<sup>1</sup>We add BatchNorm to all conv layers in VGG16 throughout this paper.

a conv kernel of one output channel. This empirical result together with our analyses in Section 4 demonstrates that there will be a large amount of accumulated noise in weights because of random initialization and noise in SGD at the initial training stage, if WD is not used.

## 4. Low-Dimension Optimization Property of SGD in BN-DNNs

In this section, the low-dimension optimization property of SGD in BatchNorm Networks is investigated. First, we demonstrate that the effective learning rate (LR) is not able to explain the good performance of weight decay. Next, our analysis on SGD shows that under some conditions the optimization only updates a subspace of a high-dimensional weights in each step. Based on this observation, we provide an explanation on the effectiveness of WD and propose a WRS regularization to achieve a similar effect as WD.

### 4.1. The Effective Learning Rate Explanation

In [50, 19], the benefit of WD on BN-DNNs is considered as a result of the increased effective learning rate (LR). We adopt the same experiment setting as in [19]. First, we train a BN-DNN with WD and record each layer’s weight norm during training. Then, we train another BN-DNN with the same neural architecture but without WD, and scale the LR according to the ratio of weight norms in the current network and the previous network, so that the effective LR of a weight is the same in the two networks. We show the test accuracy of the two VGG16 networks in Fig. 1 (as “scale lr”). The result seemingly validates the hypothesis that WD benefits generalization by increasing the effective LR. However, there are several problems in this experiment. First, it is hard to scale the LR exactly since in a certain layer the correspondence between nodes or channels of the two networks is unknown. Second, if increased LR explains the power of WD, then increasing the LR of all weights by a common value should work as well. However, the experiment in Fig. 1 shows that the uniform LR scaling cannot even match the performance of SGD without WD using normal LR. Third, we find that a regularization scheme that rescales weights (WRS) to a unit  $l_2$  norm during training achieves the same level of performance as WD. Yet the effective LR in WRS training is believed to be much smaller than that of WD training [46]. The effective LR argument is also questioned in [15], where they find that this argument cannot explain why WD only manifests its benefit when applied at the early training stage instead of later training stages (see Fig. 7). We provide our explanation on the time-dependent effect of WD in Sec. 5.

### 4.2. SGD Analysis Based on Input Feature Space

As shown in Section 3, the gradient of the empirical risk w.r.t. a weight  $\mathbf{W}_{l,j}$  is a linear combination of

$\{\partial\hat{h}_{l+1,j}^{(i)} / \partial\mathbf{W}_{l,j}\}_{i=1}^B$ . Further examining (5), we have

$$\frac{\partial\hat{h}_{l+1,j}^{(i)}}{\partial\mathbf{W}_{l,j}} = \frac{\gamma_{l,j}}{\|\mathbf{W}_{l,j}\|_{\Sigma_l^{(B)}}} \left[ (\mathbf{h}_l^{(i)} - \boldsymbol{\mu}_l^{(B)}) - t_{l,j}^{(i)} \frac{\boldsymbol{\Sigma}_l^{(B)} \mathbf{W}_{l,j}}{\|\mathbf{W}_{l,j}\|_{\Sigma_l^{(B)}}} \right].$$

Let  $\boldsymbol{\Sigma}_l^{(B)} = \mathbf{U}_l^{(B)} \boldsymbol{\Lambda}_l^{(B)} \mathbf{U}_l^{(B)T}$  be the eigendecomposition, where  $\mathbf{U}_l^{(B)}$  is the left unitary matrix whose columns are eigenvectors, and  $\boldsymbol{\Lambda}_l^{(B)}$  is the diagonal matrix of the eigenvalues. Multiplying both sides of (5) by  $(\mathbf{U}_l^{(B)})^T$ ,

$$d\mathbf{V}_{l,j} = \frac{\gamma_{l,j}}{\|\mathbf{W}_{l,j}\|_{\Sigma_l^{(B)}}} [(\mathbf{U}_l^{(B)})^T (\mathbf{h}_l^{(i)} - \boldsymbol{\mu}_l^{(B)}) - t_{l,j}^{(i)} \frac{\boldsymbol{\Lambda}_l^{(B)} \mathbf{V}_{l,j}^{(B)}}{\|\mathbf{W}_{l,j}\|_{\Sigma_l^{(B)}}}],$$

where  $\mathbf{V}_{l,j}^{(B)}$  is the mapping of  $\mathbf{W}_{l,j}$  onto the subspace spanned by input features and  $d\mathbf{V}_{l,j}$  denotes the projection of  $\partial\hat{h}_{l+1,j}^{(i)} / \partial\mathbf{W}_{l,j}$  onto the input feature span. Note that the rank of  $\boldsymbol{\Sigma}_l^{(B)} \in \mathbb{R}^{H_l \times H_l}$  is  $\min(B-1, H_l)$ , where  $H_l$  is the dimension of feature vector  $\mathbf{h}_l^{(i)}$  and  $B$  is the batch size.

Suppose that the number of data samples in this batch is smaller than the dimension of features, i.e.  $B-1 < H_l$ , then there will be  $(H_l+1-B)$  zeros eigenvalues. For example, VGG16 has many layers where the number of image patches  $B$  is far smaller than the dimension of those patches. The first term is the mapping of  $\mathbf{h}_l^{(i)} - \boldsymbol{\mu}_l^{(B)}$  onto the subspace spanned by  $\mathbf{U}_l^{(B)}$ . Suppose that the eigenvalues are in descending order, then this mini-batch has no component in the last  $(H_l+1-B)$ -dimension when projected to the space  $\mathbf{U}_l^{(B)}$ . Thus, the first term only has  $B-1$  nonzero elements. The second term is also a vector whose last  $(H_l+1-B)$  elements are zero, which is straightforward due to the  $(H_l+1-B)$  zeros eigenvalues in  $\boldsymbol{\Lambda}$ . Thus, the gradient of  $\mathbf{V}_{l,j}$  only has  $B-1$  nonzero values,

$$d\mathbf{V}_{l,j} = [(\partial\mathbf{V}_{l,j})_1, (\partial\mathbf{V}_{l,j})_2, \dots, (\partial\mathbf{V}_{l,j})_{B-1}, 0, \dots, 0].$$

In an optimization step, only  $B-1$  components of weights are updated if we observe from the data subspace. Our analysis is similar to [25], where the optimization of a one-hidden-layer NN is investigated by eigendecomposition of the input space. The difference is that here we generalize the previous result to a BN-DNN and demonstrate that the low-rank update also holds in BN layers.

It could be argued that in some layers of DNNs, the dimensionality of features is smaller than the number of feature patches in a batch. However, even if  $H_l < B-1$ , the intrinsic dimension of features  $\tilde{H}_l$  is demonstrated to be substantially lower than the dimension of their ambient space  $H_l$  [16, 1]. This low intrinsic dimension reduces the nonzero components in  $d\mathbf{V}_{l,j}$  if  $\tilde{H}_l < B-1$ , and further lowers the updated dimension by SGD. The low-rank optimization brings difficulties to the generalization of BN-DNNs since weight components orthogonal to input feature

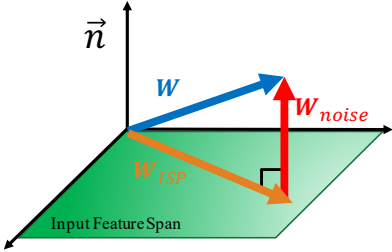


Figure 4. Weight decomposition as its input space projection (ISP) and orthogonal ISP ( $\vec{n}$ ). The 3D space represents high-dimensional feature space while the plane represents the low-dimensional span of input features. The  $W_{noise}$  is due to random initialization and stochasticity in SGD, which is outside the input feature span and cannot be eliminated in later optimization. Our analysis shows that WRS and WD help remove such noise.

spans cannot be updated by SGD, and the complexity of NN is not effectively controlled [3]. Although a BN-DNN is invariant to weight scaling, WD is still needed to penalize redundant weight components and learn a DNN with low complexity. Without WD, SGD is prone to poor generalization as a result of noise in weights [26], emerging from random initialization and stochasticity in SGD. Fig. 4 illustrates the decomposition of a weight vector into its ISP and orthogonal ISP comprising noise. Since SGD only updates weights inside the ISP, the noise will accumulate in the orthogonal space and cannot be removed in later optimization.

To validate our hypothesis, we fit a generalized Gaussian distribution (GGD) [35] to the parameter values in a convolution layer. The shape parameter  $\beta_{GG}$  of the GGD controls the tail shape of the distribution:  $\beta_{GG} = 2$  corresponds to a Gaussian distribution;  $\beta_{GG} < 2$  corresponds to a heavy-tail distribution with lower values giving fatter tails ( $\beta_{GG} = 1$  is a Laplacian);  $\beta_{GG} > 2$  gives light-tail distributions, and  $\beta_{GG} \rightarrow \infty$  yields uniform distribution around 0 (i.e., no tails). In other words, a large  $\beta_{GG}$  indicates that more kernel parameters are noise around zero, while a small  $\beta_{GG} < 2$  indicates the kernel has a more sparse structure (e.g., see Supp. B.2). Using a well-trained VGG16 on CIFAR10, we fit GGDs for kernel parameters in all 13 conv layers, and plot the  $\beta_{GG}$  versus layers in Fig. 5 before and after projecting weights to their input spans. The input spans are obtained by collecting features of all training data in each layer and computing  $U_l$  by eigendecomposition of  $\Sigma_l$ . Fig. 5 has three implications. First, from the first layer to the final layer, conv parameters become less sparse if we observe after the input span projection (ISP). Second, when we consider ISP of weights, SGD with WD leads to more sparse kernels than vanilla SGD (Fig. 5a). However, the sparsity cannot be observed from the parameter space directly (Fig. 5b). Third, weight distributions in initial layers are quite sparse even though  $B$  is much larger

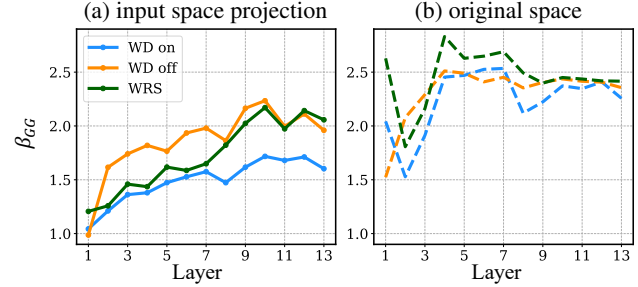


Figure 5. Shape parameter  $\beta_{GG}$  of generalized Gaussians for weights in (a) input space projection (ISP) and (b) original space, versus conv layer. WD and WRS lead to more sparse weights at early layers in the ISP instead of the original space, compared to without WD.

than their  $H_l$ 's, indicating that the intrinsic dimension  $\tilde{H}_l$  plays a more important role than the batch size.

One natural question for this low-dimension optimization property of SGD is whether the ISP of a layer varies drastically from epoch to epoch. We empirically show that despite the change of input features, SGD leads to more noise in weights compared to SGD with WD when applying ISP to weights. Fig. 6 shows the change of  $\beta_{GG}$  of projected weight parameters from 0 to 100 epochs. Combined with Fig. 5, we conclude that the sparse weight structures caused by WD are observed from their ISPs, while they cannot be observed directly from the parameter space. In Supp. B.1, we show weight parameter distributions in different epochs.

## 5. Weight Rescaling Regularization

Using our previous analyses on the noise accumulation of SGD, we propose a regularization strategy that has the same complexity control effect as WD but avoids its disadvantages in some optimization methods. Weight rescaling (WRS) consists of scaling weight vectors or conv kernels to the unit norm every  $\tau$  steps during training. Although a BN-DNN function is invariant to weight rescaling, here we demonstrate that WRS regularizes weight noise and improves generalization, while also mitigates negative influences of WD on advanced optimizers.

**WRS suppresses noise in weights in the early training stages.** Although a BN-DNN function is invariant to rescaling the weights, the optimization process is affected by the WRS operation. Recall two properties about SGD derived in previous sections: 1) one SGD step increases the  $l_2$  norm proportional to the learning rate and gradient norms; 2) one SGD step only updates a small portion of weight components inside the ISP. Thus, we conclude that when a BN-DNN is at the initial training stage, where both the learning rate and gradient norms are large, SGD will lead to several relatively large components in a weight's ISP

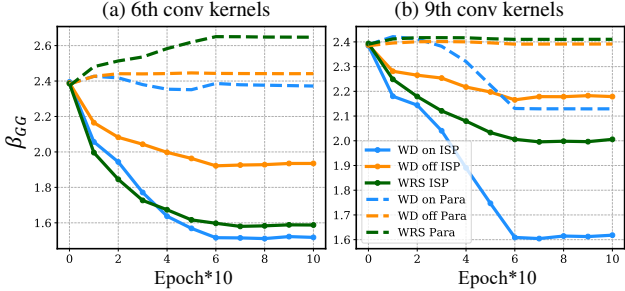


Figure 6. Shape parameters  $\beta_{GG}$  of generalized Gaussians vs. training epochs for the 6th and 9th conv kernels. Dashed lines and solid lines denote the GGD for conv kernels in parameter space (Para) and input space projection (ISP). The weight sparsity changes dramatically at early training epochs, and remains stable after 60 epochs because of learning rate decay.

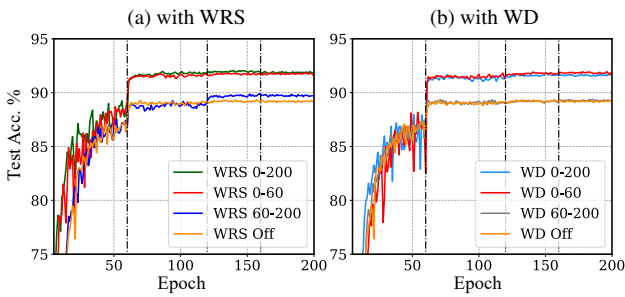


Figure 7. Training curves when using WRS and WD. Black dashed lines denote epochs at which the learning rate is decayed. The effect on generalization of both WRS and WD is time-dependent.

and renormalizing a weight in ISP to the unit norm makes larger components get larger and small components get smaller. This renormalization strategy is similar to renormalizing weights for actions in decision making, or weak classifiers in Adaboost [13, 30]. Thus, WRS suppresses small noise in weights in a different way from WD. Although the weight rescaling operation is done in the input space, the orthonormal projection does not change weight norms, and thus WRS in the input space is equivalent to WRS in the parameter space (See Supp. A.4).

To validate our hypothesis that WRS has its benefit at the initial training stage, we apply WRS in different training epochs and compare the time effect of WRS with WD in Fig. 7. In the experiment, we multiply the learning rate by 0.1 in epochs 60, 120 and 160. Similar to [15], we find that WD cannot improve generalization when applied in the later stage of training (curve for “WD 60-200”). The time-dependent effect is also observed in WRS since we cannot have the same level of performance when using WRS in only epochs 60-200. This observation corroborates our hypothesis on the mechanics of WRS. Our explanation of the time-dependent effect of WD and WRS is that the noise in weights, as a result of random initialization and stochasticity in SGD, should be suppressed in early epochs, otherwise

those noise will accumulate and construct noisy input feature spaces that cannot be mitigated by WD or WRS. Fig. 6 shows that when observed from ISP, in the 6th conv layer, WRS has a similar distribution shape to WD while in the deeper 9th layer, WRS’s distribution shape is between WD and vanilla SGD. However, if we observe from the parameter space, WRS has the least sparse weight structures in both layers. In Supp. B.2, we give the visualization of distributions for 6th conv parameters during training. Fig. 5 further demonstrates that WRS has similar sparse structures as SGD-WD in initial layers, and similar parameter distributions as vanilla SGD at final layers, indicating the network needs a sparse structure at initial layers instead of final layers to achieve better performance.

**Improved Optimization.** It is observed that WD might hurt the performance of certain optimizers, and AdamW is proposed to overcome the performance deterioration when using WD in Adam [32]. Since we show that WRS has a similar regularization effect to WD, we propose to use WRS to avoid the drawback of WD when using some complex optimizers. In Sec. 6, we show the advantage of WRS over WD in several computer vision tasks, in terms of improved generalization and convergence.

The faster convergence of WRS might come from the balanced weight norms induced by the normalization. It is known that unbalanced weights lead to poor optimization behavior in standard NNs [36]. Although a BN-DNN function is invariant to unbalanced weight norms, gradients of weights are proportional to the inverse of weight norms. If a weight has a significantly large norm compared to others, the gradient of this weight will be relatively small. Therefore, balanced weight norms in a BN-DNN give balanced gradients in SGD, benefitting the convergence rate.

**Why does the LR scaling help the network generalize, but the uniform LR scaling does not?** The multiplier in “scale lr” is approximately one at the initialization, increases dramatically in the first training stage (1-60 epochs) and then remains stable in the second training stage (after 60 epoch). Training using “scale lr” is the same as training without weight decay when the weight norms are small in the first several epochs. Then the weight norms increase according to Corollary 3.3 and LR is scaled up. The progressively increased scales make gradients in the ISP greater and effectively suppress noise resulting from previous SGD steps. This approach is opposite to WRS: WRS diminishes noise by scaling down the noise, while the LR scaling increases important components. The uniform LR scaling hurts the generalization because the scales of gradients are equivalently large throughout training so there is no regularization for redundant noise in weights. See Supp. B.1 for the visualization of scale values in the “scale lr” experiment.

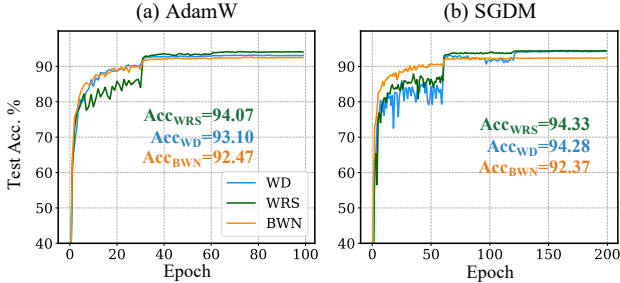


Figure 8. Learning curves of WRS, BWN and WD on ResNet18-variant and CIFAR10. WRS has the best performance even though it does not achieve the fastest convergence at early epochs.

## 6. Experiment

In this section, we demonstrate the effectiveness of BN+WRS compared to BN+WD through experiments on four computer vision tasks.

### 6.1. Image Recognition

We apply WRS to different neural architectures and image recognition datasets and compare the performance of WRS and WD. Three classical BN-DNNs, VGG16, ResNet18 [18] and WideResNet-28-10 [49], are used as our test models and CIFAR10, CIFAR100 [24] and Tiny ImageNet [9] are used as the datasets. Note that the original ResNet and WideResNet architectures have some conv layers without BN, and here we add BN for all convolution layers in this experiment to make a thorough comparison.<sup>2</sup> Since SGD often has worse performance than SGD with momentum (SGDM) or Adam, we only use SGDM and Adam in our experiment. To avoid the performance drop when using Adam and WD, we use AdamW as an alternative to Adam. For WD, we apply weight decay on all conv kernels and  $\gamma$ 's in the BN layers. For WRS, we rescale conv kernels to the unit norm every  $\tau$  optimization steps, and apply weight decay on  $\gamma$ 's in the BN layers. Note that the weight decay for  $\gamma$  does not interfere with our analyses for weights in previous sections, since we do not make any assumptions on the dynamics of  $\gamma$ . In both WRS and WD, the hyperparameter for decay is set as 5e-4 and batch size is 100.  $\tau$  is chosen from {10, 20, 40} based on their performance on the validation set. See Supp. B.2 for more details.

Table 1 shows a comparison of test accuracies between WRS and WD with various NNs, datasets, and optimization methods, where each accuracy is an average over running 3 trials. In most settings, especially for AdamW optimiza-

<sup>2</sup>In the Supp. B.2, we show that WRS also achieves better results than WD for the original ResNets in the image recognition experiment, indicating that WRS is not affected by the reduced number of BN layers in ResNets. In the other CV tasks, we do not use variants of ResNet when training with WRS and still obtain better results than WD.

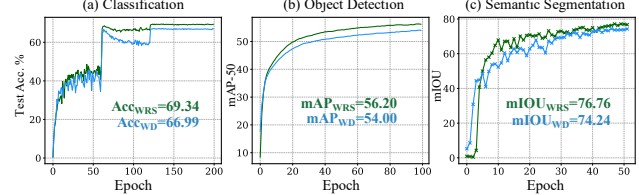


Figure 9. Learning curves of WRS and WD on different CV tasks.

tion, WRS performs better than WD in terms of test accuracy. Averaging over all datasets, architectures, and optimizers, WRS has overall higher accuracy (mean 76.9) versus WD (75.7), which is statistically significant via paired t-test,  $t(17)=3.4498$ ,  $p=0.003$ . This result demonstrates that, in general, WRS improves generalization over WD when using advanced optimizers. Fig. 9a shows the test accuracy of training WideResNet on Tiny ImageNet with WRS and WD. WRS has a clear advantage over WD in this large-scale model and dataset scenario, in terms of stable training, and better generalization. In Supp. B.2, we provide an empirical study on the hyperparameters of WRS.

WeightNorm+WD is not included as a baseline in Tab. 1 since the performance of WN is shown to be generally worse than BN+WD in image classification [14]. Fig. 8 compares WRS with bounded WN (BWN) with mean-only BN [19] and WD. Although the convergence of BWN is faster than WRS and WD at the first training stage, BWN hurts the final accuracy in general. In addition to the performance benefit, WRS is easier to implement and robust to different NN architectures compared to BWN. For example, training with BWN on VGG16 is always broken in our experiment.

### 6.2. Other Computer Vision Tasks

We next compare WRS and WD on BN-DNNs from other computer vision tasks.

**Object detection.** YOLOv3 [41] is a popular detection model with efficient training and inference. The darknet backbone [40] and YOLO head make heavy use of BN layers to stabilize the training. Thus, we empirically study the effectiveness of WRS in the object detection task by comparing the performance of training YOLOv3 with WRS and WD on the COCO dataset [29]. In WRS, we rescale a conv kernel if there is a BN layer after the convolution, and use weight decay on all other parameters. Fig. 9b shows the mAP of YOLOv3 on the validation set during training with SGDM. WRS is consistently better than WD after the first several epochs and converges faster than WD. The final mAP of WRS improves over WD by 2.2.

**Semantic segmentation.** DeepLabv3 [7] finds that BN is important to train the backbone and atrous convolution lay-

Network+Opt.	Reg.	C10	C100	Tiny
VGG16+SGDM	WD	92.24	<b>69.79</b>	57.90
	WRS	<b>92.37</b>	69.69	<b>58.28</b>
VGG16+AdamW	WD	92.40	68.02	49.14
	WRS	<b>93.32</b>	<b>68.15</b>	<b>52.15</b>
ResNet18+SGDM	WD	94.37	76.13	63.44
	WRS	<b>94.41</b>	<b>76.77</b>	<b>64.02</b>
ResNet18+AdamW	WD	93.44	72.83	<b>62.47</b>
	WRS	<b>94.26</b>	<b>75.95</b>	62.17
WideResNet+SGDM	WD	94.14	<b>80.25</b>	66.82
	WRS	<b>95.22</b>	79.95	<b>69.22</b>
WideResNet+AdamW	WD	94.17	74.97	60.57
	WRS	<b>94.59</b>	<b>78.89</b>	<b>64.03</b>

Table 1. Test accuracy of WRS and WD in the image recognition task. C10, C100, and Tiny denote CIFAR10, CIFAR100, and Tiny ImageNet. A paired t-test over all datasets, architectures, and optimizers indicates that WRS has overall higher accuracy (mean 76.9) versus WD (75.7),  $t(17)=3.4498$ ,  $p=0.003$ .

ers. As all convolution layers in DeepLabv3 are equipped with BN, we train DeepLabv3 using WRS for all conv kernels and compare that with WD. ResNet101 is chosen as the backbone of DeepLabv3 in our experiment. The network is trained on the augmented PASCAL VOC 2012 semantic segmentation dataset [12, 17] using AdamW, and the output stride is 16. Fig. 9c shows the mIOU of DeepLabv3 on the validation set during training. Our WRS achieves better performance (mIOU increase of 2.52) and faster convergence, compared to WD.

**Crowd counting.** We test WRS on crowd counting, a regression CV task. CSRNet [28] with VGG16 as the backbone is used as the model and Bayesian loss [34] is the empirical risk. The model is trained and evaluated on UCF-QNRF [21]. VGG16 is initialized by ImageNet pre-trained weights. Adam is the optimizer and batch size is 32. We train the model for 300 epochs and choose one model with the lowest mean absolute error (MAE) on the validation set. On the test set, training with WD gives an MAE of 103.84 and mean squared error (MSE) of 176.28, while WRS improves the two metrics by 7.33 and 2.48, achieving 96.51 MAE and 173.80 MSE.

## 7. Conclusion

In this paper, we theoretically analyze SGD optimization of BN-DNNs from the perspective of the training dynamics of weight norms and weight updating in a low-dimensional subspace. Based on our analyses, we explain the effect of WD as removing weight noise in the space orthogonal to the input feature span. WRS is proposed to replace WD in training with SGDM or Adam to avoid drawbacks of WD. Our empirical studies corroborate our explanation and demonstrate the effectiveness of WRS across various CV tasks, different neural architectures, and datasets. Our work can be further improved in several directions. First, it

will be significant if we could find the relationship between weight sparsity in the input feature span and generalization of DNNs. Second, we empirically show the effectiveness of WRS on ResNet but do not analyze how residual connections affect the optimization and generalization in a BN-DNN. Third, we can investigate the effect of WRS in different learning paradigms where BN is crucial to training stability and generalization, like adversarial learning [39], contrastive learning [8] and meta-learning [45].

## References

- [1] Alessio Ansuini, Alessandro Laio, Jakob H Macke, and Davide Zoccolan. Intrinsic dimension of data representations in deep neural networks. In *Advances in Neural Information Processing Systems*, pages 6111–6122, 2019. 2, 5
- [2] Sanjeev Arora, Nadav Cohen, and Elad Hazan. On the optimization of deep networks: Implicit acceleration by over-parameterization. In *International Conference on Machine Learning*, pages 244–253, 2018. 2, 3
- [3] Peter L Bartlett, Dylan J Foster, and Matus J Telgarsky. Spectrally-normalized margin bounds for neural networks. In *Advances in Neural Information Processing Systems*, pages 6240–6249, 2017. 6
- [4] Peter L Bartlett, Philip M Long, Gábor Lugosi, and Alexander Tsigler. Benign overfitting in linear regression. *Proceedings of the National Academy of Sciences*, 2020. 3
- [5] Mikhail Belkin, Siyuan Ma, and Soumik Mandal. To understand deep learning we need to understand kernel learning. In *International Conference on Machine Learning*, pages 541–549, 2018. 3
- [6] Nils Bjorck, Carla P Gomes, Bart Selman, and Kilian Q Weinberger. Understanding batch normalization. In *Advances in Neural Information Processing Systems*, pages 7694–7705, 2018. 2
- [7] Liang-Chieh Chen, George Papandreou, Florian Schroff, and Hartwig Adam. Rethinking atrous convolution for semantic image segmentation. *arXiv preprint arXiv:1706.05587*, 2017. 1, 8, 17
- [8] Ting Chen, Simon Kornblith, Mohammad Norouzi, and Geoffrey Hinton. A simple framework for contrastive learning of visual representations. *arXiv preprint arXiv:2002.05709*, 2020. 9
- [9] Jia Deng, Wei Dong, Richard Socher, Li-Jia Li, Kai Li, and Li Fei-Fei. Imagenet: A large-scale hierarchical image database. In *2009 IEEE conference on computer vision and pattern recognition*, pages 248–255. Ieee, 2009. 8
- [10] Simon S Du, Wei Hu, and Jason D Lee. Algorithmic regularization in learning deep homogeneous models: Layers are automatically balanced. In *Advances in Neural Information Processing Systems*, pages 384–395, 2018. 3
- [11] Simon S Du, Xiyu Zhai, Barnabas Poczos, and Aarti Singh. Gradient descent provably optimizes over-parameterized neural networks. In *International Conference on Learning Representations*, 2018. 2, 3
- [12] Mark Everingham, SM Ali Eslami, Luc Van Gool, Christopher KI Williams, John Winn, and Andrew Zisserman. The

PASCAL visual object classes challenge: A retrospective. *International journal of computer vision*, 111(1):98–136, 2015. 9, 17

[13] Yoav Freund and Robert E Schapire. A decision-theoretic generalization of on-line learning and an application to boosting. *Journal of computer and system sciences*, 55(1):119–139, 1997. 7

[14] Igor Gitman and Boris Ginsburg. Comparison of batch normalization and weight normalization algorithms for the large-scale image classification. *arXiv preprint arXiv:1709.08145*, 2017. 8

[15] Aditya Sharad Golatkar, Alessandro Achille, and Stefano Soatto. Time matters in regularizing deep networks: Weight decay and data augmentation affect early learning dynamics, matter little near convergence. In *Advances in Neural Information Processing Systems*, pages 10678–10688, 2019. 5, 7

[16] Sixue Gong, Vishnu Naresh Boddeti, and Anil K Jain. On the intrinsic dimensionality of image representations. In *Proceedings of the IEEE Conference on Computer Vision and Pattern Recognition*, pages 3987–3996, 2019. 2, 5

[17] Bharath Hariharan, Pablo Arbeláez, Lubomir Bourdev, Subhransu Maji, and Jitendra Malik. Semantic contours from inverse detectors. In *2011 International Conference on Computer Vision*, pages 991–998. IEEE, 2011. 9, 17

[18] Kaiming He, Xiangyu Zhang, Shaoqing Ren, and Jian Sun. Deep residual learning for image recognition. In *Proceedings of the IEEE conference on computer vision and pattern recognition*, pages 770–778, 2016. 1, 8

[19] Elad Hoffer, Ron Banner, Itay Golan, and Daniel Soudry. Norm matters: efficient and accurate normalization schemes in deep networks. In *Advances in Neural Information Processing Systems*, pages 2160–2170, 2018. 1, 2, 4, 5, 8, 16

[20] Lei Huang, Xianglong Liu, Bo Lang, and Bo Li. Projection based weight normalization for deep neural networks. *arXiv preprint arXiv:1710.02338*, 2017. 2, 3

[21] Haroon Idrees, Muhammad Tayyab, Kishan Athrey, Dong Zhang, Somaya Al-Maadeed, Nasir Rajpoot, and Mubarak Shah. Composition loss for counting, density map estimation and localization in dense crowds. In *Proceedings of the European Conference on Computer Vision (ECCV)*, pages 532–546, 2018. 9, 17

[22] Sergey Ioffe and Christian Szegedy. Batch normalization: Accelerating deep network training by reducing internal covariate shift. *arXiv preprint arXiv:1502.03167*, 2015. 1, 3

[23] Diederik P Kingma and Jimmy Ba. Adam: A method for stochastic optimization. *arXiv preprint arXiv:1412.6980*, 2014. 2

[24] Alex Krizhevsky et al. Learning multiple layers of features from tiny images. 2009. 8

[25] Anders Krogh and John A Hertz. A simple weight decay can improve generalization. In *Advances in neural information processing systems*, pages 950–957, 1992. 3, 5

[26] Xiang Li, Shuo Chen, and Jian Yang. Understanding the disharmony between weight normalization family and weight decay. In *AAAI*, pages 4715–4722, 2020. 1, 6

[27] Yuanzhi Li, Colin Wei, and Tengyu Ma. Towards explaining the regularization effect of initial large learning rate in training neural networks. In *Advances in Neural Information Processing Systems*, pages 11674–11685, 2019. 1

[28] Yuhong Li, Xiaofan Zhang, and Deming Chen. CSRnet: Dilated convolutional neural networks for understanding the highly congested scenes. In *Proceedings of the IEEE conference on computer vision and pattern recognition*, pages 1091–1100, 2018. 9, 17

[29] Tsung-Yi Lin, Michael Maire, Serge Belongie, James Hays, Pietro Perona, Deva Ramanan, Piotr Dollár, and C Lawrence Zitnick. Microsoft COCO: Common objects in context. In *European conference on computer vision*, pages 740–755. Springer, 2014. 8, 16

[30] N Littlestone and MK Warmuth. The weighted majority algorithm. In *Proceedings of the 30th Annual Symposium on Foundations of Computer Science*, pages 256–261, 1989. 7

[31] Ziquan Liu, Yufei Cui, and Antoni B Chan. Improve generalization and robustness of neural networks via weight scale shifting invariant regularizations. *arXiv preprint arXiv:2008.02965*, 2020. 2

[32] Ilya Loshchilov and Frank Hutter. Decoupled weight decay regularization. In *International Conference on Learning Representations*, 2018. 2, 7

[33] Ping Luo, Xinjiang Wang, Wenqi Shao, and Zhanglin Peng. Towards understanding regularization in batch normalization. *arXiv preprint arXiv:1809.00846*, 2018. 2

[34] Zhiheng Ma, Xing Wei, Xiaopeng Hong, and Yihong Gong. Bayesian loss for crowd count estimation with point supervision. In *Proceedings of the IEEE International Conference on Computer Vision*, pages 6142–6151, 2019. 9, 17

[35] Saralees Nadarajah. A generalized normal distribution. *Journal of Applied statistics*, 32(7):685–694, 2005. 6

[36] Behnam Neyshabur, Russ R Salakhutdinov, and Nati Srebro. Path-SGD: Path-normalized optimization in deep neural networks. In *Advances in Neural Information Processing Systems*, pages 2422–2430, 2015. 2, 7

[37] Behnam Neyshabur, Ryota Tomioka, Ruslan Salakhutdinov, and Nathan Srebro. Data-dependent path normalization in neural networks. *arXiv preprint arXiv:1511.06747*, 2015. 4

[38] Siyuan Qiao, Huiyu Wang, Chenxi Liu, Wei Shen, and Alan Yuille. Weight standardization. *arXiv preprint arXiv:1903.10520*, 2019. 3

[39] Alec Radford, Luke Metz, and Soumith Chintala. Unsupervised representation learning with deep convolutional generative adversarial networks. *arXiv preprint arXiv:1511.06434*, 2015. 9

[40] Joseph Redmon. Darknet: Open source neural networks in c, 2013. 8, 16

[41] Joseph Redmon and Ali Farhadi. YOLOv3: An incremental improvement. *arXiv preprint arXiv:1804.02767*, 2018. 1, 8, 16

[42] Tim Salimans and Durk P Kingma. Weight normalization: A simple reparameterization to accelerate training of deep neural networks. In *Advances in neural information processing systems*, pages 901–909, 2016. 1, 4

- [43] Shibani Santurkar, Dimitris Tsipras, Andrew Ilyas, and Aleksander Madry. How does batch normalization help optimization? In *Advances in Neural Information Processing Systems*, pages 2483–2493, 2018. [2](#)
- [44] Karen Simonyan and Andrew Zisserman. Very deep convolutional networks for large-scale image recognition. *arXiv preprint arXiv:1409.1556*, 2014. [4](#)
- [45] Jake Snell, Kevin Swersky, and Richard Zemel. Prototypical networks for few-shot learning. In *Advances in neural information processing systems*, pages 4077–4087, 2017. [9](#)
- [46] Twan Van Laarhoven. L2 regularization versus batch and weight normalization. *arXiv preprint arXiv:1706.05350*, 2017. [2, 4, 5](#)
- [47] Yuxin Wu and Kaiming He. Group normalization. In *Proceedings of the European conference on computer vision (ECCV)*, pages 3–19, 2018. [16](#)
- [48] Greg Yang, Jeffrey Pennington, Vinay Rao, Jascha Sohl-Dickstein, and Samuel S Schoenholz. A mean field theory of batch normalization. In *International Conference on Learning Representations*, 2018. [2](#)
- [49] Sergey Zagoruyko and Nikos Komodakis. Wide residual networks. In *BMVC*, 2016. [8](#)
- [50] Guodong Zhang, Chaoqi Wang, Bowen Xu, and Roger Grosse. Three mechanisms of weight decay regularization. In *International Conference on Learning Representations*, 2018. [1, 2, 5](#)

## A. Proof of Theorems, Corollaries and Claims

Here we provide proofs of the Theorems and Corollaries in our paper.

### A.1. Proof of Theorem 3.1

**Theorem 3.1** Suppose that we have a network as in Section 3.1, which is trained using SGD to minimize the loss  $R_{\Theta}$ , then the gradient flow of  $l_2$  norms of the weights in BatchNorm layers is zero,

$$\frac{d\|\mathbf{W}_{l,j}(t)\|_2^2}{dt} = 0. \quad (8)$$

*Proof.* Using a minibatch of data  $(\mathbf{X}^{(B)}, \mathbf{Y}^{(B)}) = \{\mathbf{x}_i, \mathbf{y}_i\}_{i=1}^B$ , we derive the gradient of the empirical loss with respect to  $\mathbf{W}_{l,j}(t)$ ,

$$\frac{\partial R_{\Theta(t)}(\mathbf{X}^{(B)}, \mathbf{Y}^{(B)})}{\partial \mathbf{W}_{l,j}(t)} = \sum_{i=1}^B \frac{\partial r^{(i)}(t)}{\partial \hat{h}_{l+1,j}^{(i)}(t)} \frac{\partial \hat{h}_{l+1,j}^{(i)}(t)}{\partial \mathbf{W}_{l,j}(t)},$$

where  $\hat{h}_{l+1,j}^i(t)$  is the  $i$ th output of BatchNorm layer. The second gradient is

$$\frac{\partial \hat{h}_{l+1,j}^{(i)}}{\partial \mathbf{W}_{l,j}} = \gamma_{l,j} \left[ \frac{\mathbf{h}_l^{(i)} - \boldsymbol{\mu}_l^{(B)}}{\|\mathbf{W}_{l,j}\|_{\boldsymbol{\Sigma}_l^{(B)}}} - \frac{\mathbf{W}_{l,j}^T(\mathbf{h}_l^{(i)} - \boldsymbol{\mu}_l^{(B)})}{\|\mathbf{W}_{l,j}\|_{\boldsymbol{\Sigma}_l^{(B)}}^3} \boldsymbol{\Sigma}_l^{(B)} \mathbf{W}_{l,j} \right], \quad (9)$$

where we omit  $t$  for clarity. This gradient is equal to

$$\frac{\partial \hat{h}_{l+1,j}^{(i)}}{\partial \mathbf{W}_{l,j}} = \gamma_{l,j} \left[ \frac{\mathbf{h}_l^{(i)} - \boldsymbol{\mu}_l^{(B)}}{(\mathbf{W}_{l,j}^T \boldsymbol{\Sigma}_l^{(B)} \mathbf{W}_{l,j})^{1/2}} - \frac{\mathbf{W}_{l,j}^T(\mathbf{h}_l^{(i)} - \boldsymbol{\mu}_l^{(B)})}{(\mathbf{W}_{l,j}^T \boldsymbol{\Sigma}_l^{(B)} \mathbf{W}_{l,j})^{3/2}} \boldsymbol{\Sigma}_l^{(B)} \mathbf{W}_{l,j} \right]. \quad (10)$$

Consider the inner product of this gradient and  $\mathbf{W}_{l,j}$ ,

$$\mathbf{W}_{l,j}^T \frac{\partial \hat{h}_{l+1,j}^{(i)}}{\partial \mathbf{W}_{l,j}} = \gamma_{l,j} \mathbf{W}_{l,j}^T \left[ \frac{\mathbf{h}_l^{(i)} - \boldsymbol{\mu}_l^{(B)}}{(\mathbf{W}_{l,j}^T \boldsymbol{\Sigma}_l^{(B)} \mathbf{W}_{l,j})^{1/2}} - \frac{\mathbf{W}_{l,j}^T(\mathbf{h}_l^{(i)} - \boldsymbol{\mu}_l^{(B)})}{(\mathbf{W}_{l,j}^T \boldsymbol{\Sigma}_l^{(B)} \mathbf{W}_{l,j})^{3/2}} \boldsymbol{\Sigma}_l^{(B)} \mathbf{W}_{l,j} \right] \quad (11)$$

$$= \gamma_{l,j} \left[ \frac{\mathbf{W}_{l,j}^T(\mathbf{h}_l^{(i)} - \boldsymbol{\mu}_l^{(B)})}{(\mathbf{W}_{l,j}^T \boldsymbol{\Sigma}_l^{(B)} \mathbf{W}_{l,j})^{1/2}} - \frac{\mathbf{W}_{l,j}^T(\mathbf{h}_l^{(i)} - \boldsymbol{\mu}_l^{(B)})}{(\mathbf{W}_{l,j}^T \boldsymbol{\Sigma}_l^{(B)} \mathbf{W}_{l,j})^{3/2}} \mathbf{W}_{l,j}^T \boldsymbol{\Sigma}_l^{(B)} \mathbf{W}_{l,j} \right] \quad (12)$$

$$= \gamma_{l,j} \left[ \frac{\mathbf{W}_{l,j}^T(\mathbf{h}_l^{(i)} - \boldsymbol{\mu}_l^{(B)})}{(\mathbf{W}_{l,j}^T \boldsymbol{\Sigma}_l^{(B)} \mathbf{W}_{l,j})^{1/2}} - \frac{\mathbf{W}_{l,j}^T(\mathbf{h}_l^{(i)} - \boldsymbol{\mu}_l^{(B)})}{(\mathbf{W}_{l,j}^T \boldsymbol{\Sigma}_l^{(B)} \mathbf{W}_{l,j})^{1/2}} \right] = 0. \quad (13)$$

Similarly, if we consider the inner product of the gradient  $\frac{\partial R_{\Theta(t)}(\mathbf{X}^{(B)}, \mathbf{Y}^{(B)})}{\partial \mathbf{W}_{l,j}(t)}$  and  $\mathbf{W}_{l,j}(t)$ , we also have

$$\left\langle \frac{\partial R_{\Theta(t)}(\mathbf{X}^{(B)}, \mathbf{Y}^{(B)})}{\partial \mathbf{W}_{l,j}(t)}, \mathbf{W}_{l,j}(t) \right\rangle = 0. \quad (14)$$

Thus, the differential equation of  $\mathbf{W}_{l,j}(t)$  is

$$\frac{d\|\mathbf{W}_{l,j}(t)\|_2^2}{dt} = -2 \left\langle \frac{\partial R_{\Theta(t)}(\mathbf{X}^{(B)}, \mathbf{Y}^{(B)})}{\partial \mathbf{W}_{l,j}(t)}, \mathbf{W}_{l,j}(t) \right\rangle = 0. \quad (15)$$

This complete the proof. Notice that we do not make any assumptions on the value of  $\gamma_{l,j}$ , so using weight decay for  $\gamma_{l,j}$  does not invalidate this theorem.

## A.2. Proof of Corollary 3.2

**Corollary 3.2** Suppose that we have a network as in Section 3.1 and the network is trained using gradient descent to minimize the loss  $R_{\Theta}$  and  $l_2$  regularizations  $\frac{\lambda}{2} \sum_{l=0}^L \|\mathbf{W}_l\|_F^2$ , then the weight  $l_2$  norm in a BatchNorm layer follows an exponential decay,

$$\|\mathbf{W}_{l,j}(t)\|_2^2 = \|\mathbf{W}_{l,j}(0)\|_2^2 \exp(-2\lambda t). \quad (16)$$

*Proof.* The ODE in SGD with weight decay is

$$\frac{d\|\mathbf{W}_{l,j}(t)\|_2^2}{dt} = -2 \left\langle \frac{\partial R_{\Theta(t)}(\mathbf{X}^{(B)}, \mathbf{Y}^{(B)})}{\partial \mathbf{W}_{l,j}(t)} + \lambda \mathbf{W}_{l,j}(t), \mathbf{W}_{l,j}(t) \right\rangle \quad (17)$$

$$= -2 \left\langle \frac{\partial R_{\Theta(t)}(\mathbf{X}^{(B)}, \mathbf{Y}^{(B)})}{\partial \mathbf{W}_{l,j}(t)}, \mathbf{W}_{l,j}(t) \right\rangle - 2 \left\langle \lambda \mathbf{W}_{l,j}(t), \mathbf{W}_{l,j}(t) \right\rangle \quad (18)$$

Using the result from Theorem 3.1 (8), we know that the first term is 0. So if there is weight decay in the training, the dynamics of weight  $l_2$  norm is

$$\frac{d\|\mathbf{W}_{l,j}(t)\|_2^2}{dt} = -2 \langle \lambda \mathbf{W}_{l,j}(t), \mathbf{W}_{l,j}(t) \rangle = -2\lambda \|\mathbf{W}_{l,j}(t)\|_2^2. \quad (19)$$

This ordinary differential equation has the form

$$\dot{x}(t) = -2\lambda x(t), x(0) = x_0, \quad (20)$$

whose solution is  $x(t) = x_0 \exp(-2\lambda t)$ . Similarly, the solution to the ODE in (19) is

$$\|\mathbf{W}_{l,j}(t)\|_2^2 = \|\mathbf{W}_{l,j}(0)\|_2^2 \exp(-2\lambda t). \quad (21)$$

This completes the proof.

## A.3. Proof of Corollary 3.3

**Corollary 3.3** Suppose that we have a network as in Section 3.1 and the network is trained by SGD to minimize  $R_{\Theta}(\mathbf{X}, \mathbf{Y})$ , then we have

$$\Delta_{l,j}(t) = \eta(t)^2 \left\| \frac{\partial R_{\Theta(t)}(\mathbf{X}^{(B)}, \mathbf{Y}^{(B)})}{\partial \mathbf{W}_{l,j}(t)} \right\|_2^2. \quad (22)$$

*Proof.* We derive the corollary as follows

$$\Delta_{l,j}(t) = \|\mathbf{W}_{l,j}(t+1)\|_2^2 - \|\mathbf{W}_{l,j}(t)\|_2^2 \quad (23)$$

$$= \|\mathbf{W}_{l,j}(t) - \eta(t) \frac{\partial R_{\Theta(t)}(\mathbf{X}^{(B)}, \mathbf{Y}^{(B)})}{\partial \mathbf{W}_{l,j}(t)}\|_2^2 - \|\mathbf{W}_{l,j}(t)\|_2^2 \quad (24)$$

$$= \|\mathbf{W}_{l,j}(t)\|_2^2 - 2\eta(t) \left\langle \mathbf{W}_{l,j}(t), \frac{\partial R_{\Theta(t)}(\mathbf{X}^{(B)}, \mathbf{Y}^{(B)})}{\partial \mathbf{W}_{l,j}(t)} \right\rangle + \quad (25)$$

$$\eta(t)^2 \left\| \frac{\partial R_{\Theta(t)}(\mathbf{X}^{(B)}, \mathbf{Y}^{(B)})}{\partial \mathbf{W}_{l,j}(t)} \right\|_2^2 - \|\mathbf{W}_{l,j}(t)\|_2^2. \quad (26)$$

Note that in Theorem 3.1, we do not use the continuous-time property when deriving (14), and thus (14) still holds in the discrete-time domain. Thus, we have  $\left\langle \mathbf{W}_{l,j}(t), \frac{\partial R_{\Theta(t)}(\mathbf{X}^{(B)}, \mathbf{Y}^{(B)})}{\partial \mathbf{W}_{l,j}(t)} \right\rangle = 0$ , and substituting yields (21).

## A.4. Weight Rescaling in Parameter Space and Input Feature Space

Assume that we have a weight vector  $\mathbf{W}_{l,j}$  and its projection into the input feature span  $\mathbf{V}_{l,j} = \mathbf{U}_l^T \mathbf{W}_{l,j}$ . Our analysis shows that  $\mathbf{V}_{l,j}$  has many small noisy components because of the random initialization and stochasticity in SGD, and some

large components as a result of increased  $l_2$  norms. So if we rescale  $\mathbf{V}_{l,j}$  to unit norm, then the small components in  $\mathbf{V}_{l,j}$  are suppressed. Suppose that we rescale  $\mathbf{V}_{l,j}$ ,

$$\tilde{\mathbf{V}}_{l,j} = \frac{\mathbf{V}_{l,j}}{\|\mathbf{V}_{l,j}\|}. \quad (27)$$

Then project  $\mathbf{V}_{l,j}$  back to the parameter space,

$$\tilde{\mathbf{W}}_{l,j} = \mathbf{U}_l \tilde{\mathbf{V}}_{l,j} = \mathbf{U}_l \frac{\mathbf{V}_{l,j}}{\|\mathbf{V}_{l,j}\|} = \mathbf{U}_l \frac{\mathbf{U}_l^T \mathbf{W}_{l,j}}{\|\mathbf{V}_{l,j}\|} = \frac{\mathbf{W}_{l,j}}{\|\mathbf{V}_{l,j}\|} = \frac{\mathbf{W}_{l,j}}{\|\mathbf{W}_{l,j}\|}, \quad (28)$$

where  $\|\mathbf{W}_{l,j}\| = \|\mathbf{V}_{l,j}\|$  since  $\mathbf{U}_l$  is the left squared matrix in the eigendecomposition of a squared matrix  $\Sigma_l$  and the orthonormal projection  $\mathbf{U}_l$  does not change the vector norm. Thus, rescaling a weight to unit norm is equivalent to rescaling its projection onto the input span to unit norm.

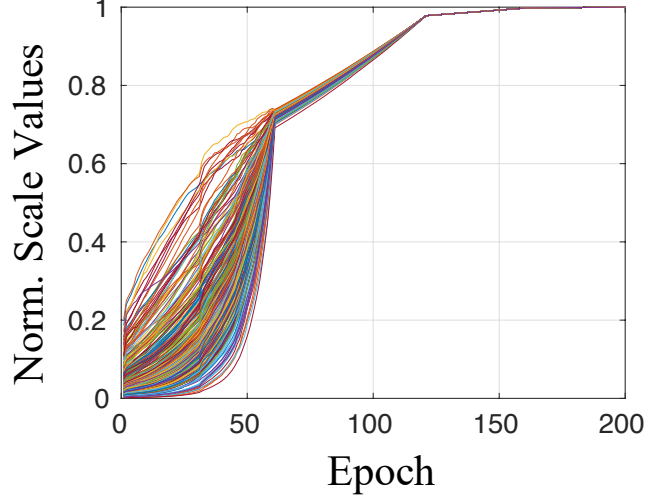


Figure S1. Learning rate scale values of 6th conv layer in VGG16 using the scale lr training scheme. To better visualize the trend, we normalize the scales to  $[0, 1]$ . Each line represents a conv kernel of one channel. It shows that the learning rate is scaled larger and larger at early training epochs while remain stable at later epochs.

## A.5. Convolution Neural Networks

As we explain in the main paper, convolution neural networks are special cases of fully-connected neural networks. Now we show that the theorem and corollaries still hold in CNNs with BatchNorm. A weight in a MLP  $\mathbf{W}_l \in \mathbb{R}^{H_l \times H_{l+1}}$  corresponds to a convolution kernel  $\mathbf{W}_l^{(K)} \in \mathbb{R}^{K_l \times K_l \times C_{l,i} \times C_{l,o}}$  in a CNN, where  $K_l$  is the size of conv kernel,  $C_{l,i}$  and  $C_{l,o}$  are the number of input and output channels. The BatchNorm for one neuron in a MLP corresponds to the BatchNorm for one conv channel in a CNN. If we use  $\mathbf{W}_{l,j}^{(K)} \in \mathbb{R}^{K_l \times K_l \times C_{l,i} \times 1}$ ,  $j = 1, \dots, C_{l,o}$  to denote the conv kernel for  $j$ th output channel and replace  $\mathbf{W}_{l,j}$  with  $\mathbf{W}_{l,j}^{(K)}$  in previous sections, our derivations also holds. The only difference is that a conv kernel is applied multiple times while a weight is multiplied once for one input point. So some summation terms need to be rewritten as a sum over input image patches. For example, the gradient of empirical risk with respect to the conv kernel  $\mathbf{W}_{l,j}^{(K)}$  is

$$\frac{\partial R_{\Theta(t)}(\mathbf{X}^{(B)}, \mathbf{Y}^{(B)})}{\partial \mathbf{W}_{l,j}^{(K)}(t)} = \sum_{i=1}^B \sum_{m=1}^{S_{l+1}} \frac{\partial r^{(i)}(t)}{\partial \hat{h}_{l+1,m,j}^{(i)}(t)} \frac{\partial \hat{h}_{l+1,m,j}^{(i)}(t)}{\partial \mathbf{W}_{l,j}^{(K)}(t)}, \quad (29)$$

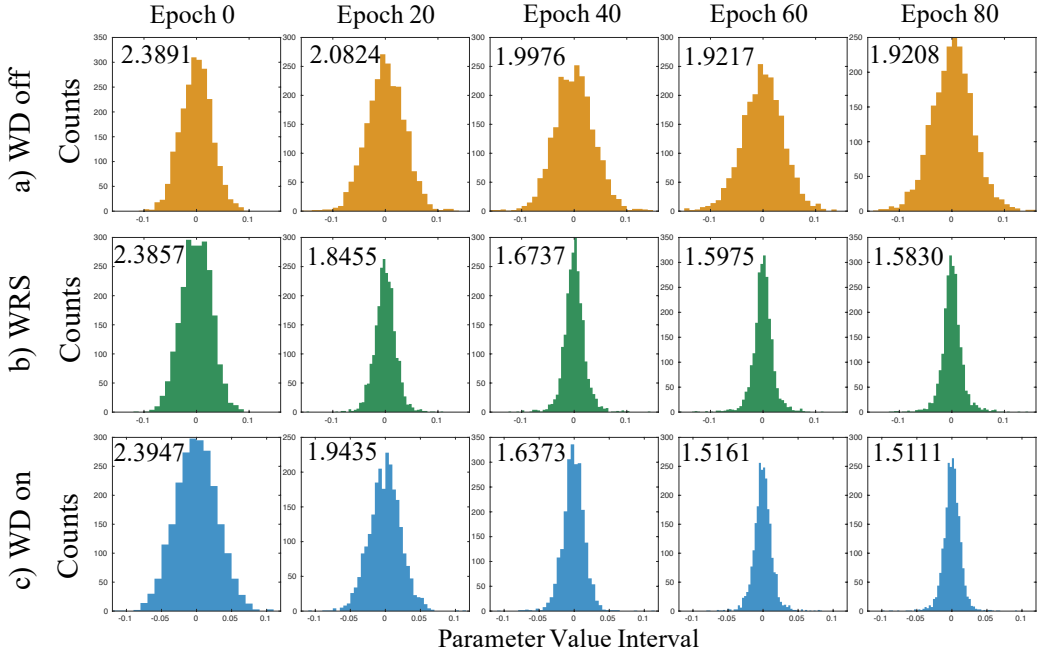


Figure S2. Change of parameter distributions during training after input span projection of the 6th conv parameters, when training with a) WD off, b) WRS and c) WD. The number in each plot denotes the shape parameter  $\beta_{GG}$  of the fit generalized Gaussian.

where  $S_{l+1}$  is the number features in one channel of  $(l+1)$ th layer. The second gradient is

$$\frac{\partial \hat{h}_{l+1,m,j}^{(i)}}{\partial \mathbf{W}_{l,j}^{(\mathcal{K})}} = \gamma_{l,j} \left[ \frac{\mathbf{h}_l^{(i)} - \boldsymbol{\mu}_l^{(B)}}{((\mathbf{W}_{l,j}^{(\mathcal{K})})^T \boldsymbol{\Sigma}_l^{(B)} \mathbf{W}_{l,j}^{(\mathcal{K})})^{1/2}} - \frac{\mathbf{W}_{l,j}^{(\mathcal{K})T} (\mathbf{h}_l^{(i)} - \boldsymbol{\mu}_l^{(B)})}{((\mathbf{W}_{l,j}^{(\mathcal{K})})^T \boldsymbol{\Sigma}_l^{(B)} \mathbf{W}_{l,j}^{(\mathcal{K})})^{3/2}} \boldsymbol{\Sigma}_l^{(B)} \mathbf{W}_{l,j}^{(\mathcal{K})} \right], \quad (30)$$

where  $\mathbf{h}_l^{(i)}$  is the image/feature patch for its output  $\hat{h}_{l+1,m,j}^{(i)}$ ,  $\boldsymbol{\mu}_l^{(B)}$  and  $\boldsymbol{\Sigma}_l^{(B)}$  are the mean and covariance computed on image/feature patches for the convolution. We can multiply  $\mathbf{W}_{l,j}^{(\mathcal{K})}$  with the gradient and get the same result as Theorem 3.1 for CNNs. Corollary 3.2 and 3.3 can also be easily derived for CNNs.

## B. More on Empirical Studies

We describe details in our experiment and provide more experimental results.

### B.1. The Effective Learning Rate Explanation

In Fig. S1, we show the learning rate scale ratios in one convolution layer of VGG16 during training without WD and scaling the learning rate to keep the effective learning rate the same as a VGG16 with WD. It demonstrates that the scale ratios change dramatically at the first 60 epochs while keep stable after this period. As we explain in the main paper, the drastically increased learning rate at early training epochs has the effect of suppressing weight noise. So this training scheme achieves the same performance as training with WD. Fig. S2 shows the change of histograms of projected weight parameters from 0 to 100 epochs, together with their GGD shape parameters. Both WRS and WD lead to sparse structures in conv kernels.

### B.2. Image Recognition

We use 3 neural architectures (VGG16, ResNet18 and WideResNet-28-10) and 3 datasets (CIFAR10, CIFAR100 and Tiny ImageNet). In all experiments of image recognition, we use a batch size of 100. When training with WRS, we rescale all weight vectors including the output layer. Although the output is not invariant to weight rescaling, the prediction is not affected by the weight scale in the classification problem. We describe the details of each scenario here.

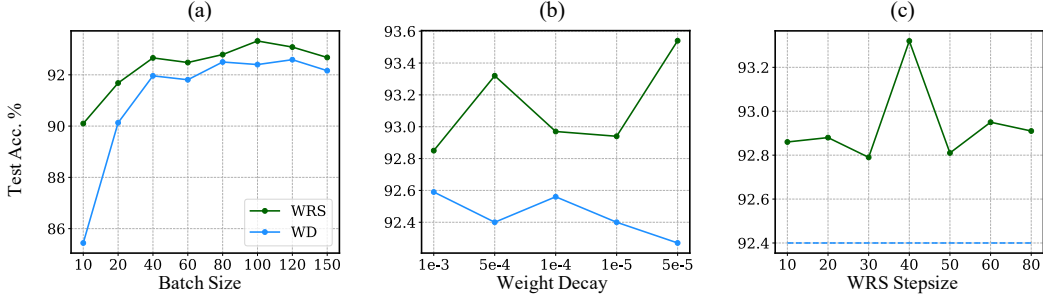


Figure S3. Empirical study of hyperparameter sensitivity. The change of test accuracy with respect to: a) Batch Size; b) Weight Decay parameter; and c) Stepsize in WRS. The blue dashed line in c) denotes the WD baseline. WRS stepsize  $\tau$  means the weight vectors are renormalized to the unit norm every  $\tau$  optimization steps. Weight decay with WRS refers to WD on the gamma parameters in BN layers.

For CIFAR10 and CIFAR100, we use the same data preprocessing procedure: 1) normalize pixel values to  $[0, 1]$ , 2) apply random horizontal flipping, random brightness, random contrast, random hue, random saturation and crop images after zero-padding  $32 \times 32$  images to  $38 \times 38$  ones. For Tiny ImageNet, we use the similar data preprocessing procedure but zero-pad  $64 \times 64$  images to  $72 \times 72$  before random cropping.

In VGG16, as we explain in the main paper, every convolution layers are followed by a BatchNorm layer. In SGDM+WD and SGDM+WRS, we train VGG16 for 200 epochs and set the initial learning rate as 0.1, which is multiplied by 0.1 at 60, 120 and 160 epoch. Dropout is not used during training. In AdamW+WD and all 3 datasets, we also train it for 200 epochs and decay the learning rate at 60, 120 and 160 epoch, but use an initial learning rate 0.001. In AdamW+WRS and all 3 datasets, we train the network for 100 epochs and decay the learning rate at 30, 60 and 80 epoch, with the same initial learning rate 0.001. We find that AdamW+WRS only needs 100 epochs to achieve the same performance of AdamW+WD training for 200 epochs, indicating a faster convergence of WRS regularization.

We use a variant of ResNet18 to do the experiment in the main paper, where each convolution layer is followed by a BatchNorm layer. In SGDM+WD, SGDM+WRS and AdamW+WD, we use the training parameters of VGG16 for ResNet18. In AdamW+WRS on CIFAR10 and CIFAR100, we train the network for 100 epochs and decay the learning rate at 30, 60 and 80 epoch, with the same initial learning rate 0.001. But in the Tiny ImageNet, we choose to train 200 epochs as in AdamW+WD to have better performance and a fair comparison with AdamW+WD. In Table S1, we show the stepsize we use in training with WRS. Note that we set the weight decay hyperparameter  $\lambda = 5e-4$  in both WRS and WD. In Table S2, we show the performance of WRS and WD using the original ResNet18 architecture. In the original ResNet18, the network function is not invariant to rescaling weights since there are several conv layers without BatchNorm. But the empirical result shows that those single convolution layers without BatchNorm do not affect the performance of WRS.

In WideResNet-28-10, we train 200 epochs in SGDM and AdamW, except in AdamW+WRS on CIFAR10 where we again train 100 epochs and use the same learning rate decay schedule as before. All other training parameters are the same as in the previous ResNet18 experiment.

Bounded WN [19] is implemented based on the code in their paper. Following the original implementation, weight decay is only used in the final fully-connected layer and mean-only BatchNorm is used for all conv layers. The initial learning rate, weight decay parameter and learning rate decay is the same as WRS and WD.

We empirically investigate the sensitivity of WRS to hyperparameters and compare with WD in the VGG16+AdamW and CIFAR10 experiment setting in Fig. S3. WRS achieves always better performance under different hyperparameter settings. Interestingly, WRS improves the performance especially when the batch size is decreased, which is known to hurt the performance of BN [47].

### B.3. Object Detection

We use YOLOv3 [41] as the model in the object detection task because of its heavy use of BatchNorm layers and faster training and inference. The original DarkNet53 [40] trained by ImageNet was chosen to initialize the backbone. We trained the network by 100 epochs with 0.01 initial learning rate and 8 batch size. The learning rate would fall by cosine schedule. The optimizer was SGDM with 0.0005 weight decay. The input size was setting to (320, 640) and we use mAP@0.5 as the evaluation metrics. We use COCO 2014 dataset [29], which includes 82,783 training images, 40,504 validation images and 80 classes. The training is on 117,263 images from training and validation set, and the evaluation is on 5,000 validation images. WRS has a stepsize of 10. Fig. S4 shows mAP, precision, recall and F score of WRS and WD.

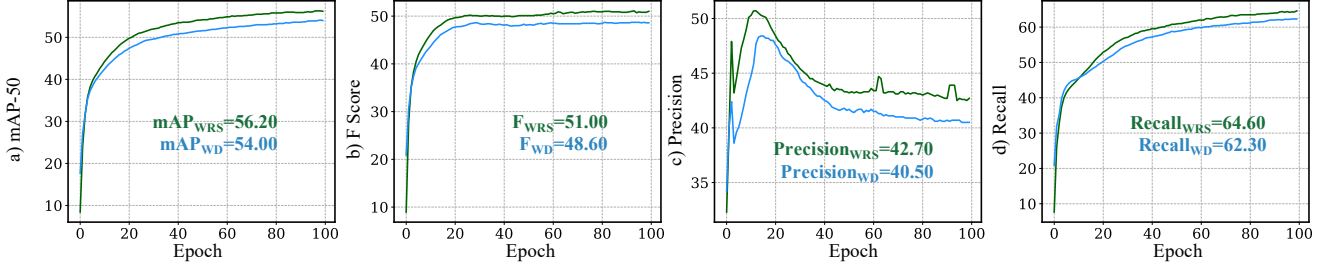


Figure S4. Comparison of a) mAP-50, b) F score, c) Precision, and d) Recall when training YOLOv3 with WRS and WD.

Network+Opt.	Reg.	C10	C100	Tiny
VGG16+SGDM	WRS	40	40	40
VGG16+AdamW	WRS	40	40	40
ResNet18+SGDM	WRS	20	10	40
ResNet18+AdamW	WRS	40	10	40
WideResNet+SGDM	WRS	40	40	40
WideResNet+AdamW	WRS	40	40	40

Table S1. Stepsize of WRS in the main paper Table 1.

Network+Opt.	Reg.	C10	C100	Tiny
ResNet18+SGDM	WD	94.14	74.92	63.03
	WRS	94.33	75.75	63.16
ResNet18+AdamW	WD	93.46	71.31	61.22
	WRS	93.77	76.32	61.70
WideResNet+SGDM	WD	95.43	79.85	66.63
	WRS	94.99	79.72	68.05
WideResNet+AdamW	WD	94.10	75.46	60.76
	WRS	94.57	79.30	63.89

Table S2. Test accuracy of original ResNet architectures. All experiments in this table use a stepsize 40 in WRS and  $\lambda = 5e-4$  in weight decay.

#### B.4. Semantic Segmentation

DeepLabv3 is used in the semantic segmentation task since it has a BatchNorm layer after every convolution layer and these BatchNorm layers turn out to be essential to the training and generalization of DeepLabv3 [7]. We use ResNet101 as the backbone and initialize it with weights pretrained on ImageNet and train DeepLabv3 using AdamW optimizer. Batch size is 10, initial learning rate is 1e-4, weight decay is 2e-4 and learning rate is scheduled as polynomial function where the end learning rate is 1e-6. The output stride is set as 16. The model is trained for 52 epochs. WRS uses a stepsize of 10. We use the augmented PASCAL VOC 2012 semantic segmentation dataset [12, 17]. There are 10,582 training images and 1,449 validation images. We use the mean Intersection Over Union (mIOU) metric for semantic segmentation in this experiment.

#### B.5. Crowd Counting

We test the performance of WRS in this regression CV task. CSRNet [28] is used as the model, where all convolution layers except for the output one are equipped with BN. So WRS is used for all conv layers before the output. VGG16 is chosen as the backbone, which is initialized by an ImageNet pretrained model. We minimize the Bayesian loss [34] in this experiment. UCF-QNRF [21] is the dataset, containing 1201 training images and 334 test images. WD and WRS use the same weight decay parameter (1e-4) and learning rate (1e-4). The batch size is 32 and cropping size is 512. WRS uses a stepsize of 1. The model is trained for 300 epochs. No learning rate decay is used throughout the training. We split the training set into training and validation images and choose the model with the best MAE on validation images as our final model.